The Post-2020 Surge in Global Atmospheric Methane Observed in Ground-based Observations

Jennifer Wu[1], Sherry Luo[1], Zhao-Cheng Zeng[2], Alex J. Turner[3], Debra Wunch[4], Omaira E. García[5], Frank Hase[6], Rigel Kivi[7], Hirofumi Ohyama[8], Isamu Morino[8], Ralf Sussmann[9], Markus Rettinger[9], Yao Té[10], Nicholas M. Deutscher[11], David W.T. Griffith[11], Kei Shiomi[12], Cheng Liu[13,14], Justus Notholt[15], Laura T. Iraci[16], David F. Pollard[17], Thornsten Warneke[18],Coleen Roehl[1], Thomas J. Pongetti[19], Stanley P. Sander[19], Yuk L. Yung[1]

[1]Division of Geological and Planetary Sciences, California Institute of Technology, Pasadena, California, USA, [2]School of Earth and Space Sciences, Peking University, Beijing, China, [3]University of Washington, [4]Department of Physics, University of Toronto, Toronto, Canada, [5]Izaña Atmospheric Research Center (IARC), State Meteorological Agency of Spain (AEMet), Santa Cruz de Tenerife, 38001, Spain, [6]Karlsruhe Institute of Technology (KIT), Institute of Meteorology and Climate Research (IMKASF), 76021 Karlsruhe, Germany, [7]Space and Earth Observation Centre, Finnish Meteorological Institute, Finland, [8]Earth System Division, National Institute for Environmental Studies (NIES), Tsukuba, Ibaraki, Japan, [9]Karlsruhe Institute of Technology (KIT), Institute of Meteorology and Climate Research (IMK-IFU), Garmisch-Partenkirchen, Germany,[10]Sorbonne Université, CNRS, MONARIS, UMR8233, F-75005 Paris, France, [11]Centre for Atmospheric Chemistry, Environmental Futures Research Centre, School of Earth, Atmospheric and Life Sciences, University of Wollongong, Wollongong, NSW, Australia, [12]Earth Observation Research Center, Japan Aerospace Exploration Agency (JAXA/EORC), [13]Department of Precision Machinery and Precision Instrumentation, University of Science and Technology of China, Hefei 230026, China, [14]Key Laboratory of Environmental Optics and Technology, Anhui Institute of Optics and Fine Mechanics, Hefei Institutes of Physical Science, Chinese Academy of Sciences, Hefei 230031, China, [15]Institute of Environmental Physics, University of Bremen, [16]Earth Science Division, NASA Ames Research Center, Moffett Field, California, USA, [17]National Institute of Water and Atmospheric Research Ltd (NIWA), Lauder, New Zealand, [18]Institute of Environmental Physics, University of Bremen, Bremen, Germany, [19]Jet Propulsion Laboratory, California Institute of Technology

Corresponding author: Jennifer Wu (wu.jennifer3643@gmail.com)

Key Points:

- Global atmospheric methane increased sharply in 2020; California shows a rise in methane at four times the rate of previous years.
- TCCON data shows that the methane rise is approximately uniform globally.
- The latest data from 2022 suggest a deceleration in the methane growth rate to the pre-2020 growth rate.

Abstract

Methane (CH_4) is a potent greenhouse gas with high radiative forcing and a relatively short atmospheric lifetime of around a decade. We used a decade-long dataset (2011-2022) from the Fourier transform spectrometer at the California Laboratory for Atmospheric Remote Sensing (CLARS-FTS) to quantify a dramatic increase in methane observed in 2020. We report an increase of 1.13 ppb/month starting in 2020 until the end of 2021, compared to a growth rate of 0.345 ppb/month from 2016 to 2019. The observed increase in methane concentrations in 2020 is of significant concern due to its potential contribution to global warming. The Total Carbon Column Observing Network (TCCON) is then used to examine the global geospatial variability of the increase in methane. The results suggest an approximately uniform rise in methane globally. Finally, results from a two-box model used to simulate atmospheric chemical processes of methane production and loss indicate that changes in OH alone are insufficient to explain the rise in atmospheric methane. Encouragingly, recent data from 2022 suggest a deceleration in the methane growth rate, indicating a potential slowdown in the methane increase observed in 2020.

Plain Language Summary

In 2020, there was a significant increase in methane, a powerful greenhouse gas. We studied data from 2011 to 2022, specifically using the California Laboratory for Atmospheric Remote Sensing. The methane levels rose sharply in 2020, increasing by 1.13 parts per billion per month, compared to a lower rate from 2016 to 2019. This rise is concerning for global warming. Our global analysis using the Total Carbon Column Observing Network shows a widespread increase in methane. Additionally, our box model results indicate that changes in OH alone can't explain the surge in methane. But there's some good news: the latest data from 2022 shows that the increase in methane might be slowing down.

1 Introduction

Atmospheric methane (CH_4) is a potent greenhouse gas with approximately 80 times the global warming potential of carbon dioxide (CO_2) over a 20-year timeframe (IPCC, 2021). Due to its relatively short atmospheric lifetime of around ten years, reducing methane emissions can have an immediate effect on slowing global warming. Urban regions, such as the Los Angeles (LA) Basin, have been shown to be major emitters of methane primarily due to leaky natural gas infrastructure (Wennberg et al., 2012; Wunch et al., 2016). In addition to leakage from urban infrastructure, other sources like oil and natural gas production also contribute to atmospheric methane increases (Hausmann et al., 2016). In an effort to slow down global warming, California implemented Senate Bill 1383 in 2016, mandating a 40 % reduction in CH_4 emissions below 2013 levels by 2030.

The year 2020 presented a unique opportunity to study the impact of human activity on atmospheric CH_4. The global COVID-19 pandemic triggered widespread lockdowns, significantly altering human behavior and reducing emissions of various pollutants, including nitrogen oxides (NO_X), CO_2, and CH_4 (e.g., Laughner et al., 2021). However, NOAA's preliminary analysis revealed a surprising outcome: a record-breaking annual increase of 15 ppb in atmospheric CH_4 (Kiest, 2021).

This unexpected surge has ignited debate about the underlying causes. While Stevenson et al. (2021) attributed it to reductions in NO_X emissions and subsequent increase in CH_4

lifetime, Qu et al. (2022) and Peng et al. (2022) highlighted the role of increased wetland emissions. Feng et al. (2022) further proposed a dominant contribution from tropical sources. Despite these valuable insights, the lack of consensus on the dominant driver for the 2020 anomaly reflects the complexity of methane dynamics (e.g., Sussmann et al., 2012).

This study contributes to the ongoing discussion by utilizing a unique approach for analyzing the 2020 CH_4 surge and its spatial variability. We leverage two critical datasets: (1) The California Laboratory for Atmospheric Remote Sensing Fourier Transform Spectrometer (CLARS-FTS) data: Beginning in 2011, CLARS-FTS provides long-term, continuous measurements of CH_4 capturing the background troposphere above the planetary boundary layer (PBL). This unique perspective allows us to isolate and analyze changes independent of local surface influences. (2) The Total Carbon Column Observing Network (TCCON) data: TCCON offers comprehensive CH_4 measurements across multiple global sites, enabling us to investigate the spatial distribution of the 2020 surge and identify potential cobtributing regions.

By analyzing these datasets and utilizing a box model used to simulate atmospheric chemical processes of methane production and loss, we aim to (1) precisely quantify the spatiotemporal dynamics of the 2020 CH_4 increase, and (2) identify potential contributing factors to the increase.

Our novel approach and detailed analysis will provide valuable insights into the complex factors influencing contemporary CH_4 dynamics. This knowledge is crucial for informing effective emission reduction strategies and ultimately mitigating the harmful impacts of atmospheric CH_4 on our planet's climate.

2 Materials and Methods

2.1 CLARS-FTS Dataset

This study utilizes a unique dataset from the California Laboratory for Atmospheric Remote Sensing Fourier transform Spectrometer (CLARS-FTS), an instrument operated by NASA's Jet Propulsion Laboratory. Located atop Mt. Wilson, California, at an altitude of 1673 m, CLARS-FTS offers a vantage point overlooking the LA Basin. It captures near-infrared solar absorption spectra by pointing toward 33 different surface reflection points. These spectra are then converted into column-averaged dry-air mole fractions of various greenhouse gases (XGHG), including carbon dioxide (XCO_2), methane (XCH_4), carbon monoxide (XCO), and nitrous oxide (XN_2O). The measurements have been acquired multiple times daily for each target location since September 2011. For detailed information on the algorithm used for converting slant column densities to dry-air column mixing ratios and instrument specifications, refer to Fu et al. (2014).

CLARS-FTS operates in two measurement modes: the Spectralon Viewing Observations (SVO) and the Los Angeles Basin Surveys (LABS). The former records the background greenhouse gas concentrations of the free troposphere above the instrument by pointing at a Spectralon target on the rooftop of the observatory, while the latter records scattered infrared radiation from target locations across the viewing area, which spans from the San Fernando Valley (western Los Angeles County) in the west to the Inland Empire (San Bernardino and Riverside Counties) in the east and Orange County in the south. The names and locations of the reflection points are given in Wong et al. (2015). This study utilizes methane data obtained using the SVO mode because PBL emissions captured by the LABS measurements confound the interpretation of the free tropospheric variability.

CLARS-FTS boasts a high degree of precision and resolution for its CH_4 measurements. Under ideal conditions, it can achieve a precision of 0.3 to 0.5 ppb for dry mixing ratios of CH_4. Additionally, its spectral resolution of 0.12 cm^{-1} allows for accurate and detailed identification of spectral features related to atmospheric CH_4 (Fu et al., 2014).

2.2 TCCON Dataset

This study also examines methane data from the Total Carbon Column Observing Network (TCCON), which is a global network of ground-based Fourier transform spectrometers that measure spectra of direct sunlight in the short-wave infrared region of the spectrum. Measurements cannot be taken during conditions of limited sunlight, such as at night or under heavy cloud cover. This limitation is similar to that of the CLARS-FTS, which relies on reflected sunlight.

Total column dry-air mole fractions of CO_2, CO, CH_4, N_2O, and other species are retrieved from the spectra using a software suite called GGG (Wunch et al., 2011), and represent the amount of the species of interest in the atmospheric column above the TCCON site. The GGG open-source software package is used by every station in the network to process data, minimizing biases between sites and ensuring easy dissemination of software improvements throughout the network. GGG utilizes GFIT, the same retrieval algorithm as CLARS-FTS, to derive slant column densities from absorption spectra.

As of 2023, TCCON comprises 30 sites worldwide, including at least one station on every continent except Antarctica and Africa. The overall objectives of the TCCON include improving the understanding of the carbon cycle and validating satellite retrievals by providing a reliable and robust ground-based dataset that adheres to stringent precision and accuracy requirements.

TCCON instruments also offer high precision and resolution for their methane measurements. Under ideal conditions, they can achieve a precision of 0.1 to 0.2 ppb for column averaged dry mole fractions of methane. Additionally, their spectral resolution of 0.02 cm^{-1} allows for accurate and detailed retrieval of atmospheric CH_4 information.

This study analyzed the CH_4 time series for 20 out of the available TCCON sites because we limited our analyses to sites for which there were at least five years of available data, encompassing the period of interest (2020 to 2021). The 20 TCCON sites span the globe, with clusters in Europe (Bremen, Garmisch, Karlsruhe, Ny-Ålesund, Orléans, Paris, and Sodankylä), North America (East Trout Lake, Edwards, Park Falls, Pasadena, and Lamont), and Asia (Hefei, Rikubetsu, Saga, and Tsukuba). These sites are primarily concentrated in the Northern hemisphere, with three in the Southern hemisphere (Darwin, Lauder, and Wollongong). Within these 20 sites, data gaps can be caused by lack of sunlight (including cloudy conditions or polar night) or instrument malfunctions. On average, the XCH_4 time series at each TCCON site have no data in 13% of the months since their measurements began.

2.3 Removing Seasonal and Long-Term Trends

To identify anomalies or deviations that are not accounted for by regular seasonal patterns or long-term trends that are well-documented in literature (He et al., 2019; Zeng et al., 2023), this study employs a methodology to remove the cyclical variations and overall trend of XCH_4 from each time series. A statistical model that consists of a linear component and a seasonal component consisting of harmonic functions is fitted to the data in each XCH_4 time series from 2016 to 2019 to model the seasonal cycle and long-term trend. The model is given by:

$$M(t) = \alpha_0 + \alpha_1 * t + \beta_1 * \sin(2\pi t) + \beta_2 * \cos(2\pi t) + \beta_3 * \sin(4\pi t) + \beta_4 * \cos(4\pi t) \qquad (1)$$

where α_{0-1} are the coefficients for the linear component, and β_{1-4} are the coefficients for the seasonal component. To ensure the accuracy and relevance of the analysis for the post-2020 period of interest, XCH_4 data from 2016 to 2019 are utilized to capture the conditions preceding the target period. The predicted values based on the model, representing the seasonal cycle and long-term trend of methane, are depicted by the red line in Figure 1.

The process of determining and removing the seasonal cycle and long-term trend of methane is repeated for each TCCON station analyzed in this study. By removing these expected variations, the study aims to highlight and investigate deviations from the regular patterns, enabling the identification and examination of anomalous methane concentrations that may be indicative of specific events or emission sources. The standard errors of the fitted model parameters are also calculated.

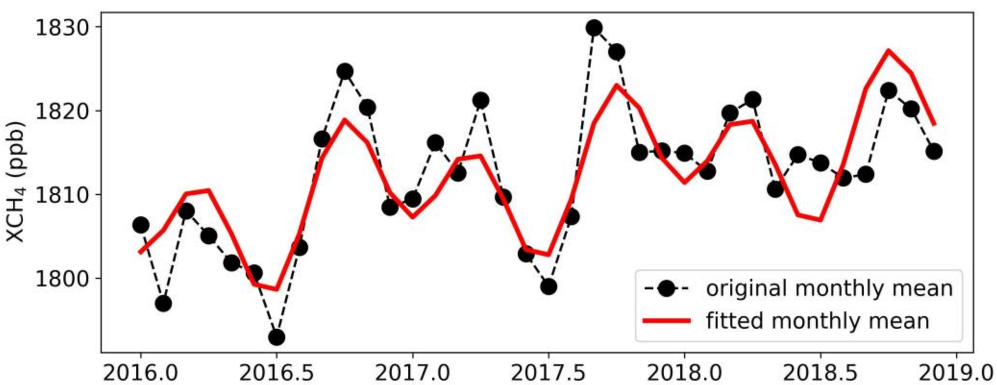

Figure 1. Comparison of original monthly mean data and fitted monthly mean of methane data from the SVO mode of CLARS-FTS using linear trend and harmonics. The figure displays the original monthly mean data (black line) and the fitted monthly mean obtained using a model incorporating both linear trend and harmonics (red line).

2.4 Estimating the Post-2020 Methane Growth Rate Using Linear Regression

In order to investigate the methane trends beyond the year 2020, a weighted linear regression analysis was conducted, using the standard deviations of each monthly mean as the weights. The methane time series data from 2020 to the end of 2021 were utilized for this analysis, and the slopes obtained from the linear regression analyses were used to represent the methane growth rate in ppb/month in each location. The availability of data past 2020 varies for each site, with some sites having more recent updates than others. For consistency, a fixed time period of the beginning of 2020 to the end of 2021 was used to compute the linear regression for all TCCON sites and CLARS-FTS. The uncertainties of the linear regression parameters were also calculated.

2.5 Box Model

A two-box model (Turner et al., 2019) with the inclusion of a coupled methane–carbon monoxide–hydroxyl radical (CH_4-CO-OH) system (Prather, 1994) was employed here to complement the impacts of changes in OH level on methane. This two-box model incorporates northern and southern hemispheres and simulates annual hemispheric concentrations of target species with a 1-year timescale for inter-hemispheric transport. Associated details of this two-box model, including target species, inversion methods and chemical reactions, can be found in Turner et al. (2017) and Nguyen et al. (2020). Even though some impacts of atmospheric processes cannot be accurately described in the box model, the well-reproduced methane stabilization and renewed growth periods in Turner et al. (2017) still present the advantages of this box model in simulating decadal trends of atmospheric methane and hydroxyl.

Thus, in response to the OH level changes resulting from COVID-19 lockdowns, a series of sensitivity tests were conducted using the box model, involving reductions in OH ranging from 2% to 5%. Furthermore, in order to assess additional impacts of methane emissions, other three tests involving changes in emissions under a 3% reduction in OH are also performed (Miyazaki et al., 2021). Note that all tests were made only for one year from 2020 to 2021, coinciding with the major COVID-19 lockdown periods.

3 Results

3.1 CLARS-FTS

Figure 2 depicts the raw monthly means of XCH_4 as captured by CLARS-FTS in the SVO mode. The raw data shows a clear seasonal cycle, with peak concentrations in winter and minimums in summer. An upward trend in XCH_4 is also evident throughout the time series. These observed trends and variability form the basis for the deseasonalized and detrended time series analysis presented in Figure 3.

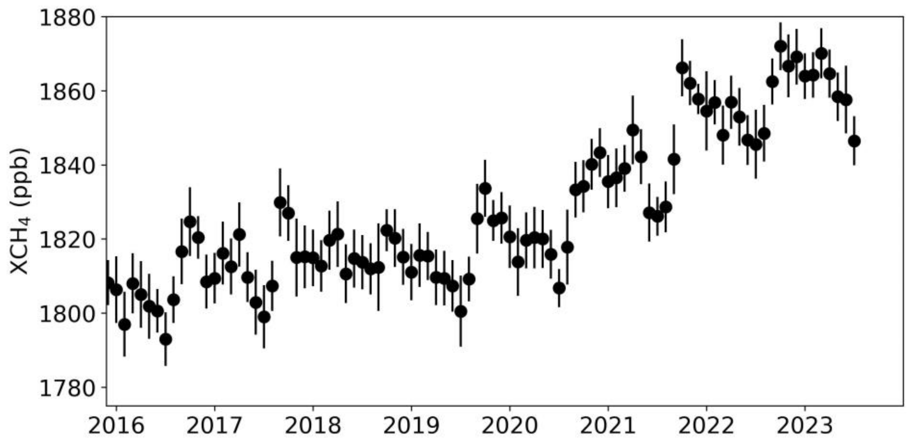

Figure 2. Monthly means of XCH_4 measured by CLARS-FTS in the SVO mode from 2016 to mid-2023. The figure provides a visual representation of the raw data, capturing the natural variability and trends in CH_4 concentrations before any deseasonalization and detrending procedures are applied.

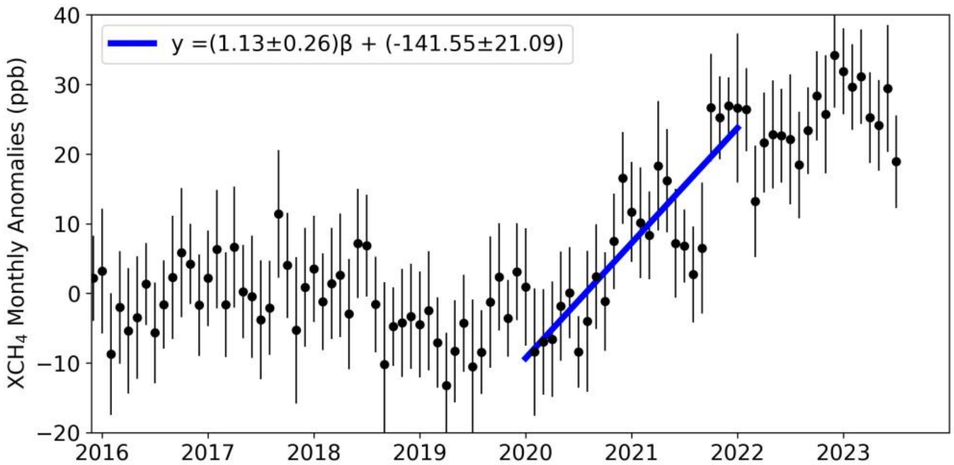

Figure 3. The deseasonalized and detrended time series of methane as measured by CLARS-FTS in the SVO mode. Error bars represent one standard deviation of the mean. The blue line represents the linear regression line.

The deseasonalized and detrended XCH_4 time series recorded by CLARS-FTS in the SVO mode is depicted in Figure 3. The linear regression analysis conducted on the 2020 to 2021 time period yielded a slope of 1.13±0.26 ppb/month, indicating a significant positive trend with a correlation coefficient of 0.69. This growth rate is consistent with the 1.16±0.21 ppb/month growth rate observed at the nearby TCCON site in Pasadena, falling within the error bars of both measurements. While this consistency indicates strong agreement between the two datasets, it is important to note that TCCON and CLARS-FTS have different viewing geometries. TCCON measures the total atmospheric column above the instrument, encompassing the planetary boundary layer (PBL), while the CLARS-FTS SVO mode measures only the portion above the PBL. This difference could potentially influence the comparison due to varying sensitivities to emission sources within the PBL. The 2020-2021 XCH_4 growth rate observed by CLARS-FTS in the SVO mode approximately 3 times higher than the 0.345±0.087 ppb/month rate observed during 2016-2019 based on the Fourier regression analysis in Section 2.3. It is worth noting that the rate of increase appears to decrease after 2022.

3.2 TCCON

This section explores the global footprint of the post-2020 XCH_4 surge observed in Figure 3. The full deseasonalized and detrended CH_4 time series for the 20 TCCON sites are included in Appendix A. Figure 4 depicts one of these time series after deseasonalizing and detrending for the TCCON station in Pasadena, California. Figure 5 presents a world map showcasing the spatial variation of the XCH_4 increase. Visually, the XCH_4 time series in Appendix A appear to show a potential stabilization or slight decrease in the rate of increase following 2022. However, further analysis and continued monitoring are needed to confirm this observation and determine if this represents a sustained change in the long-term trend.

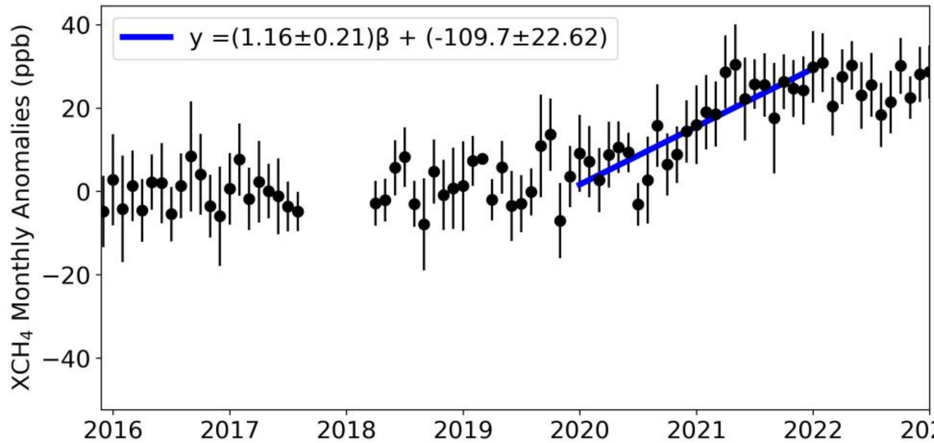

Figure 4. The deseasonalized and detrended time series of CH_4 measured by the TCCON station at Pasadena, California. Error bars represent one standard deviation of the mean. The blue line is derived by linear regression of the data from 2020 to 2021.

Figure 4 shows a strong increase in XCH_4 during the 2020-2021 period observed by the TCCON station at Pasadena, California. There is a notable gap in the data record at the end of 2017. The absence of data at the end of 2017 may impact the deseasonalization and detrending analysis because data from 2016-2019 are used to perform the fitting. The optimal parameters derived from the Fourier fitting and their associated 1-sigma uncertainties are reported in Table S1. The same deceleration of the methane surge seen in CLARS-FTS's data starting in 2022 is seen in Figure 4.

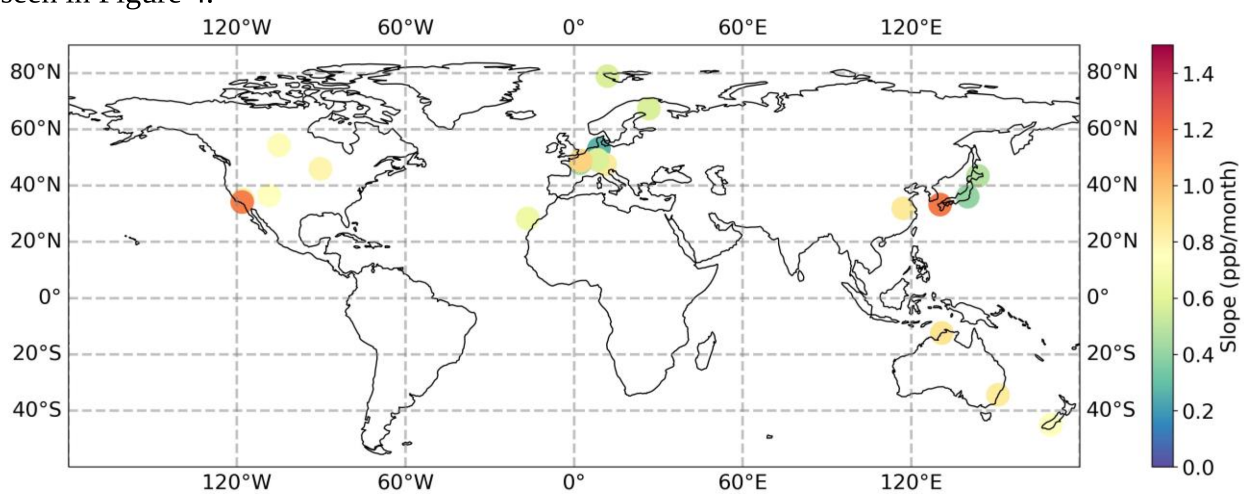

Figure 5. Global distribution of XCH_4 growth rates. The figure displays a world map with color-coded markers representing the methane growth rates derived by the slopes of the linear regression lines fit to data from 2020 to 2021. The colorbar on the right side of the map indicates the range of slope values, ranging from 0 to 1.5 ppb/month.

The methane growth rates reported in Table 1 are all positive, indicating that the increase in methane was widespread across the globe and not limited to a single region. Overall, the narrow range of methane growth rates from 0.27 to 1.17 ppb/month suggests that the increase of methane in 2020 to 2021 was approximately uniform across the globe. The TCCON site at Bremen, Germany reports an unusually low methane growth rate of 0.27 ppb/month. However, examination of the time series in Figure A1 reveals a high degree of data unavailability, which can significantly impact the reliability of the growth rate estimate. Consequently, this low growth rate might not be representative of the actual methane trends at Bremen, Germany.

Table 1. *XCH_4 Growth Rates Estimated by Linear Regression of 2020-2021 Data at each TCCON Site*

Site	Location (Lat, Lon)	Growth Rate (ppb/month)	Uncertainty (ppb/month)	Data Reference
Karlsruhe	49.1, 8.44	0.58	0.13	Hase et al. (2023)
Izaña	28.3, -16.48	0.65	0.14	Garcia et al. (2023)
Hefei	31.91, 117.17	0.85	0.15	Liu et al. (2023)
Paris	48.85, 2.36	0.93	0.16	Té et al. (2023)
Edwards	34.96, -117.88	0.84	0.17	Iraci et al. (2023)
Garmisch	47.48, 11.06	1.08	0.17	Sussman and Rettinger (2023)
Bremen	53.1, 8.85	0.27	0.19	Notholt et al. (2023)
Park Falls	45.94, -90.27	0.80	0.19	Wennberg et al. (2023)
Lauder	-45.05, 169.68	0.75	0.20	Pollard et al. (2024)
Lamont	36.5, -108.48	0.75	0.20	Wennberg et al. (2022)
Sodankyla	67.37, 26.63	0.57	0.20	Kivi et al. (2023)
Pasadena	34.14, -118.13	1.16	0.21	Wennberg et al. (2022)
Saga	33.24, 130.29	1.17	0.21	Shiomi et al. (2023)
East Trout Lake	54.35, -104.99	0.77	0.22	Wunch et al. (2023)
Darwin	-12.43, 130.29	0.92	0.23	Deutscher et al. (2024)
Orléans	47.97, 2.11	0.44	0.24	Warneke et al. (2024)
Wollongong	-34.41, 150.88	0.84	0.25	Deutscher et al. (2023)
Ny Ålesund	78.9, 11.9	0.57	0.28	Buschmann et al. (2023)
Rikubetsu	43.46, 143.77	0.48	0.35	Morino et al. (2023a)
Tsukuba	36.05, 140.12	0.40	0.49	Morino et al. (2023b)

3.3 Box Model

In comparison to the deseasonalized and detrended methane data obtained from CLARS-FTS, seasonal trends of the box model results were also removed. This was accomplished using the same Linear Trend and Harmonics approach, also with corresponding data from 2016 to 2019 serving as the conditions preceding the target period. As shown in Figure 6, overall, increases in methane concentrations are quite noticeable across all sensitivity tests. However, the growth rates vary in different tests. Methane emissions play the dominant role as the greatest increase in emission leads to the highest growth rate in methane. Since the primary removal process for methane is oxidation by hydroxyl radicals (OH), a scenario excluding emissions changes implies that higher methane growth rates would directly correspond to larger decreases in OH levels.

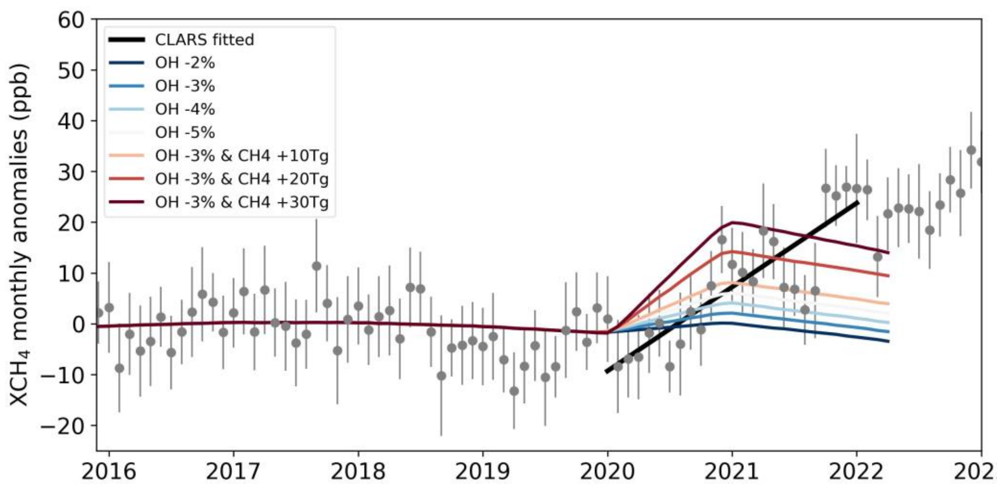

Figure 6. The deseasonalized and detrended time series of methane concentrations from sensitivity tests based on the box model, along with the methane measured by CLARS-FTS in the SVO mode and corresponding linear regression line in black.

It is important to note that these simulations were conducted for the period 2020-2021 to specifically investigate the impact of COVID-19 lockdowns on XCH_4. This limited timeframe likely explains why the model shows a decrease in XCH_4 after 2021, whereas the CLARS-FTS data shows a continued increase.

Additionally, when compared with CLARS-FTS where its growth rate is represented with the fitted line through linear regression analysis, it is evident that the growth rates of methane from the box model are consistently lower. More importantly, the growth of methane in the box model ceases after 2021 without the continuous jump of methane as observed in CLARS-FTS after 2021. Therefore, in addition to reductions in OH levels, there should exist other factors contributing to the sustained rise in methane for the post-lockdown periods.

4 Conclusions

We used ground-based observations, CLARS-FTS and TCCON, to investigate the 2020 surge in atmospheric CH_4 concentrations. CLARS-FTS recorded a strong increase in XCH_4 above the planetary boundary layer of 1.13±0.26 ppb/month from 2020 to the end of 2021. Analyses of the CH_4 time series from twenty TCCON sites suggest that the increase in atmospheric XCH_4 was approximately uniform globally. The dramatic rise in XCH_4 was global in scale and not limited to a single region.

Notably, recent data from 2022 suggest a deceleration in this growth rate. This emerging trend highlights the need for continued monitoring to understand the long-term dynamics of atmospheric methane.

Though reductions in OH due to COVID-19 lockdowns may have contributed to the rise in methane during 2020 and beyond, they do not appear to be the sole drivers, as methane concentrations continue to rise even after the lockdown periods in some cases. Our box model results support this idea as decreases in OH alone are not enough to match the rise in methane observed by CLARS-FTS.

In conclusion, further work needs to be done to untangle the causes behind the dramatic increase in methane. Continued monitoring, integrating more datasets, and utilizing models can add clarity to the factors contributing to the 2020 surge in methane. The response of atmospheric methane to the COVID-19 lockdowns emphasizes the need to consider complex atmospheric chemistry feedbacks when developing and implementing climate change policies.

Acknowledgments

We acknowledge Dr. Paul Wennberg for his instrumental role in securing funding through the Linde Center grant (GPS.LRFUNDS-3.12-ENDOW.STANBACK) that supported this research. We are also grateful to Dr. Wennberg for providing access to TCCON data from the Lamont, Park Falls, and Pasadena sites, and for his valuable comments.The TCCON sites at Rikubetsu and Tsukuba are supported in part by the GOSAT series project. The Paris TCCON site has received funding from Sorbonne Université, the French center CNRS and the French agency CNES. Darwin and Wollongong TCCON stations are supported by ARC grants DP160100598, LE0668470, DP140101552, DP110103118, and DP0879468 and Darwin through NASA grants NAG5-12247 and NNG05-GD07G.

Open Research

CLARS-FTS XCH_4 data are publicly available at https://data.caltech.edu/records/254mc-zpg74. (https://doi.org/10.22002/D1.1985). TCCON data are available at https://tccondata.org/. The codes and data used to generate the figures in this manuscript can be found at https://web.gps.caltech.edu/~zcz/doc/Code+Data_Wuetal_ESS/.

Appendix A

This appendix includes the full deseasonalized and detrended methane time series for each TCCON station.

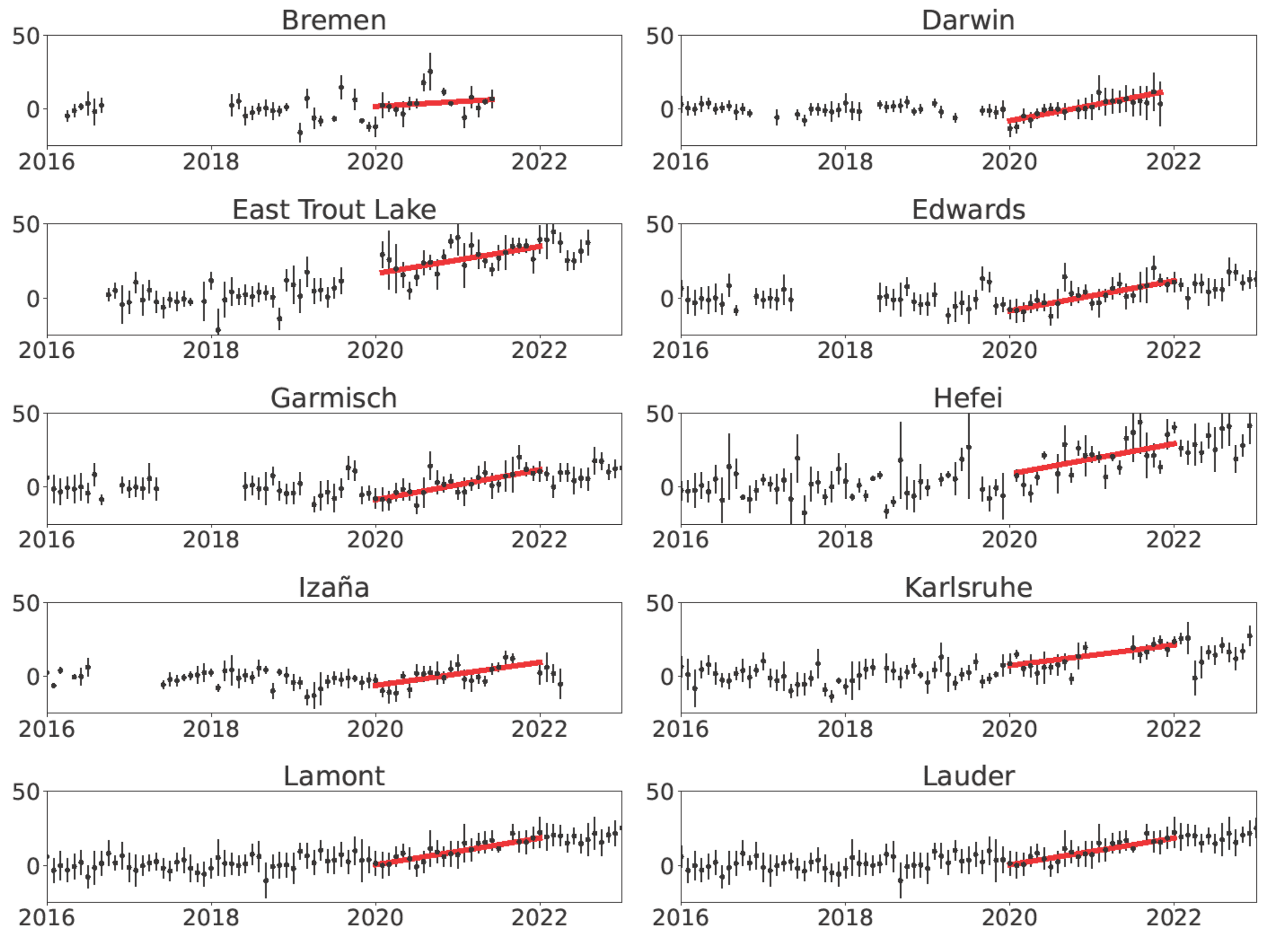

Figure A1. The deseasonalized and detrended time series of CH_4 concentrations for 10 TCCON sites. Each panel depicts data for an individual site, labeled accordingly. The superimposed red lines represent linear regressions for the 2020-2021 period, highlighting the upward trends in CH_4 concentrations. The slopes and their respective uncertainties are reported in Table 1.

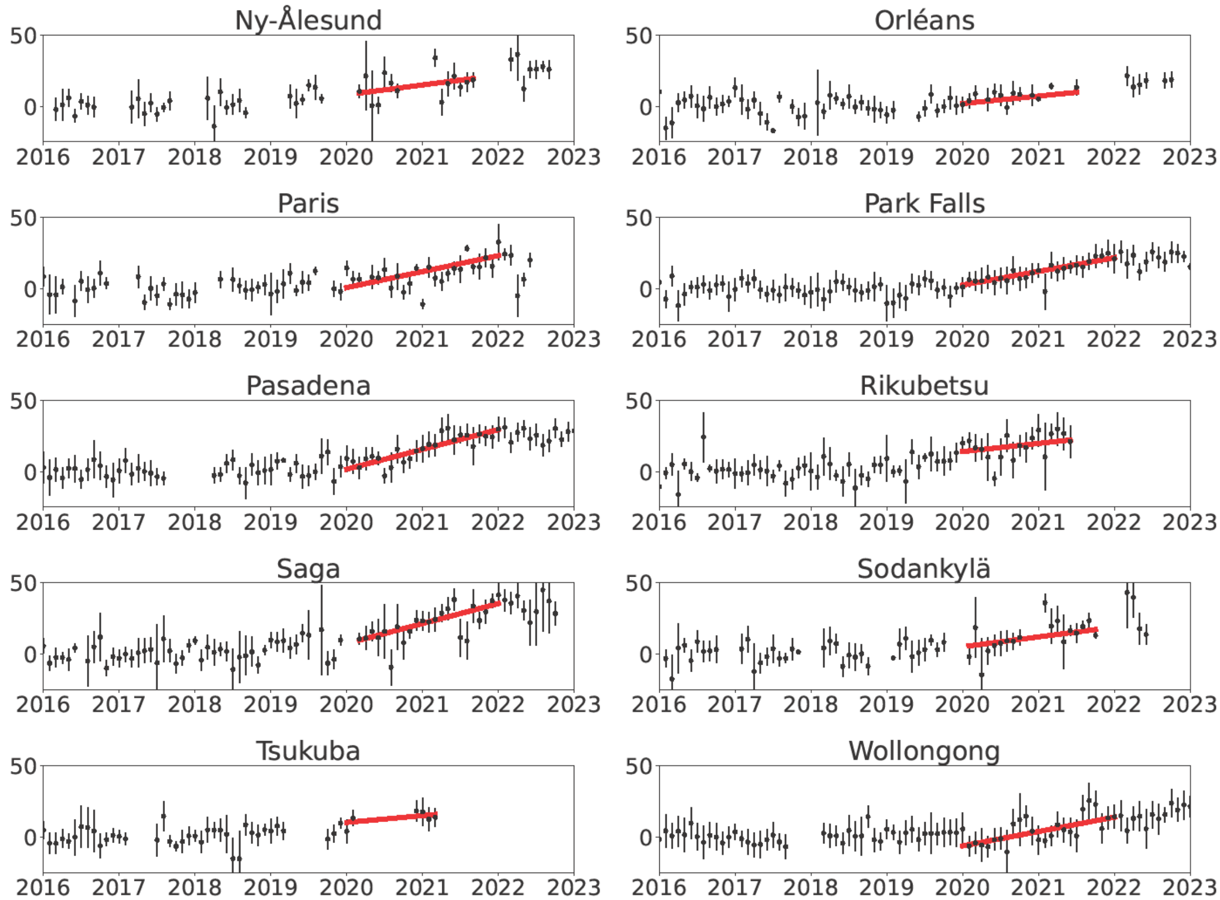

Figure A2. The deseasonalized and detrended time series of CH_4 concentrations for 10 additional TCCON sites. Each panel depicts data for an individual site, labeled accordingly. The superimposed red lines represent linear regressions for the 2020-2021 period, highlighting the upward trends in CH_4 concentrations. The slopes and their respective uncertainties are reported in Table 1.

References

Buschmann, M., Petri, C., Palm, M., Warneke, T., & Notholt, J. (2023). TCCON data from Ny-Ålesund, Svalbard (NO), Release GGG2020.R0 (Version R0) [Data set]. CaltechDATA. https://doi.org/10.14291/TCCON.GGG2020.NYALESUND01.R0

Deutscher, N. M., Griffith, D. W. T., Paton-Walsh, C., Jones, N. B., Velazco, V. A., Wilson, S. R., et al. (2023). TCCON data from Wollongong (AU), Release GGG2020.R0 (Version R0) [Data set]. CaltechDATA. https://doi.org/10.14291/TCCON.GGG2020.WOLLONGONG01.R0

Deutscher, N. M., Griffith, D. W. T., Paton-Walsh, C., Velazco, V. A., Wennberg, P. O., Blavier, J.-F., et al. (2024). TCCON data from Darwin (AU), Release GGG2020.R0 (Version R0) [Data set]. CaltechDATA. https://doi.org/10.14291/TCCON.GGG2020.DARWIN01.R0

Feng, L., Palmer, P. I., Parker, R. J., Lunt, M. F., & Boesch, H. (2022). *Methane emissions responsible for record-breaking atmospheric methane growth rates in 2020 and 2021* (preprint). Gases/Remote Sensing/Troposphere/Chemistry (chemical composition and reactions). https://doi.org/10.5194/acp-2022-425

Fu, D., Pongetti, T. J., Blavier, J.-F. L., Crawford, T. J., Manatt, K. S., Toon, G. C., et al. (2014). Near-infrared remote sensing of Los Angeles trace gas distributions from a mountaintop site. *Atmospheric Measurement Techniques*, *7*(3), 713–729. https://doi.org/10.5194/amt-7-713-2014

García, O. E., Schneider, M., Herkommer, B., Gross, J., Hase, F., Blumenstock, T., & Sepúlveda, E. (2023). TCCON data from Izana (ES), Release GGG2020.R1 (Version R1) [Data set]. CaltechDATA. https://doi.org/10.14291/TCCON.GGG2020.IZANA01.R1

Hase, F., Herkommer, B., Groß, J., Blumenstock, T., Kiel, M.ä., & Dohe, S. (2023). TCCON data from Karlsruhe (DE), Release GGG2020.R1 (Version R1) [Data set]. CaltechDATA. https://doi.org/10.14291/TCCON.GGG2020.KARLSRUHE01.R1

Hausmann, P., Sussmann, R., & Smale, D. (2016). Contribution of oil and natural gas production to renewed increase in atmospheric methane (2007–2014): top–down estimate from ethane and methane column observations. *Atmospheric Chemistry and Physics*, *16*(5), 3227–3244. https://doi.org/10.5194/acp-16-3227-2016

He, L., Zeng, Z.-C., Pongetti, T. J., Wong, C., Liang, J., Gurney, K. R., et al. (2019). Atmospheric Methane Emissions Correlate With Natural Gas Consumption From Residential and Commercial Sectors in Los Angeles. *Geophysical Research Letters*, *46*(14), 8563–8571. https://doi.org/10.1029/2019GL083400

Intergovernmental Panel on Climate Change (IPCC). (2021). *IPCC Fifth Assessment Report: Climate Change 2021: The Physical Science Basis*. Retrieved from https://www.ipcc.ch/report/ar6/wg1/

Iraci, L. T., Podolske, J. R., Roehl, C., Wennberg, P. O., Blavier, J.-F., Allen, N., et al. (2023). TCCON data from Edwards (US), Release GGG2020.R0 (Version R0) [Data set]. CaltechDATA. https://doi.org/10.14291/TCCON.GGG2020.EDWARDS01.R0

Kiest, K. (2021, April 7). Despite pandemic shutdowns, carbon dioxide and methane surged in 2020. Retrieved July 9, 2023, from https://research.noaa.gov/2021/04/07/despite-pandemic-shutdowns-carbon-dioxide-and-methane-surged-in-2020/

Kivi, R., Heikkinen, P., & Kyrö, E. (2023). TCCON data from Sodankylä (FI), Release GGG2020.R0 (Version R0) [Data set]. CaltechDATA. https://doi.org/10.14291/TCCON.GGG2020.SODANKYLA01.R0

Laughner, J. L., Neu, J. L., Schimel, D., Wennberg, P. O., Barsanti, K., Bowman, K. W., et al. (2021). Societal shifts due to COVID-19 reveal large-scale complexities and feedbacks between atmospheric chemistry and climate change. *Proceedings of the National Academy of Sciences*, *118*(46), e2109481118. https://doi.org/10.1073/pnas.2109481118

Liu, C., Wang, W., Sun, Y., & Shan, C. (2023). TCCON data from Hefei (PRC), Release GGG2020.R0 (Version R0) [Data set]. CaltechDATA. https://doi.org/10.14291/TCCON.GGG2020.HEFEI01.R0

Miyazaki, K., Bowman, K., Sekiya, T., Takigawa, M., Neu, J. L., Sudo, K., et al. (2021). Global tropospheric ozone responses to reduced NO_x emissions linked to the COVID-19 worldwide lockdowns. *Science Advances*, *7*(24), eabf7460. https://doi.org/10.1126/sciadv.abf7460

Morino, I., Ohyama, H., Hori, A., & Ikegami, H. (2023a). TCCON data from Rikubetsu (JP), Release GGG2020.R0 (Version R0) [Data set]. CaltechDATA. https://doi.org/10.14291/TCCON.GGG2020.RIKUBETSU01.R0

Morino, I., Ohyama, H., Hori, A., & Ikegami, H. (2023b). TCCON data from Tsukuba (JP), 125HR, Release GGG2020.R0 (Version R0) [Data set]. CaltechDATA. https://doi.org/10.14291/TCCON.GGG2020.TSUKUBA02.R0

Nguyen, N. H., Turner, A. J., Yin, Y., Prather, M. J., & Frankenberg, C. (2020). Effects of Chemical Feedbacks on Decadal Methane Emissions Estimates. *Geophysical Research Letters*, *47*(3), e2019GL085706. https://doi.org/10.1029/2019GL085706

Notholt, J., Petri, C., Warneke, T., & Buschmann, M. (2023). TCCON data from Bremen (DE), Release GGG2020.R0 (Version R0) [Data set]. CaltechDATA. https://doi.org/10.14291/TCCON.GGG2020.BREMEN01.R0

Peng, S., Lin, X., Thompson, R. L., Xi, Y., Liu, G., Hauglustaine, D., et al. (2022). Wetland emission and atmospheric sink changes explain methane growth in 2020. *Nature*, *612*(7940), 477–482. https://doi.org/10.1038/s41586-022-05447-w

Pollard, D. F., Robinson, J., & Shiona, H. (2024). TCCON data from Lauder (NZ), Release GGG2020.R0 (Version R0) [Data set]. CaltechDATA. https://doi.org/10.14291/TCCON.GGG2020.LAUDER03.R0

Prather, M. J. (1994). Lifetimes and eigenstates in atmospheric chemistry. *Geophysical Research Letters*, *21*(9), 801–804. https://doi.org/10.1029/94GL00840

Qu, Z., Jacob, D. J., Zhang, Y., Shen, L., Varon, D. J., Lu, X., et al. (2022). Attribution of the 2020 surge in atmospheric methane by inverse analysis of GOSAT observations. *Environmental Research Letters*, *17*(9), 094003. https://doi.org/10.1088/1748-9326/ac8754

Stanley Sander, Thomas Pongetti, Zhao-Cheng Zeng, & Yuk Yung. (2021). CLARS-FTS XGHGs Dataset (2011-2020) (Version 1.0) [Data set]. https://doi.org/10.22002/D1.1985

Shiomi, K., Kawakami, S., Ohyama, H., Arai, K., Okumura, H., Ikegami, H., & Usami, M. (2023). TCCON data from Saga (JP), Release GGG2020.R0 (Version R0) [Data set]. CaltechDATA. https://doi.org/10.14291/TCCON.GGG2020.SAGA01.R0

Stevenson, D., Derwent, R., Wild, O., & Collins, W. (2021). *COVID-19 lockdown NO_x emission reductions can explain most of the coincident increase in global atmospheric methane* (preprint). Gases/Atmospheric Modelling/Troposphere/Chemistry (chemical composition and reactions). https://doi.org/10.5194/acp-2021-604

Sussmann, R., & Rettinger, M. (2023). TCCON data from Garmisch (DE), Release GGG2020.R0 (Version R0) [Data set]. CaltechDATA. https://doi.org/10.14291/TCCON.GGG2020.GARMISCH01.R0

Sussmann, R., Forster, F., Rettinger, M., & Bousquet, P. (2012). Renewed methane increase for five years (2007–2011) observed by solar FTIR spectrometry. *Atmospheric Chemistry and Physics*, *12*(11), 4885–4891. https://doi.org/10.5194/acp-12-4885-2012

Té, Y., Jeseck, P., & Janssen, C. (2023). TCCON data from Paris (FR), Release GGG2020.R0 (Version R0) [Data set]. CaltechDATA. https://doi.org/10.14291/TCCON.GGG2020.PARIS01.R0

Turner, A. J., Frankenberg, C., Wennberg, P. O., & Jacob, D. J. (2017). Ambiguity in the causes for decadal trends in atmospheric methane and hydroxyl. *Proceedings of the National Academy of Sciences*, *114*(21), 5367–5372. https://doi.org/10.1073/pnas.1616020114

Turner, A. J., Frankenberg, C., & Kort, E. A. (2019). Interpreting contemporary trends in atmospheric methane. *Proceedings of the National Academy of Sciences*, *116*(8), 2805–2813. https://doi.org/10.1073/pnas.1814297116

Warneke, T., Petri, C., Notholt, J., & Buschmann, M. (2024). TCCON data from Orléans (FR), Release GGG2020.R0 (Version R0) [Data set]. CaltechDATA. https://doi.org/10.14291/TCCON.GGG2020.ORLEANS01.R0

Wennberg, P. O., Mui, W., Wunch, D., Kort, E. A., Blake, D. R., Atlas, E. L., et al. (2012). On the Sources of Methane to the Los Angeles Atmosphere. *Environmental Science & Technology*, *46*(17), 9282–9289. https://doi.org/10.1021/es301138y

Wennberg, P. O., Roehl, C.M., Wunch, D, Blavier, J.-F., Toon, G. C., Allen, N. T., et al. (2022). TCCON data from Caltech (US), Release GGG2020.R0 (Version R0) [Data set]. CaltechDATA. https://doi.org/10.14291/TCCON.GGG2020.PASADENA01.R0

Wennberg, P. O., Roehl, C. M., Wunch, D., Toon, G. C., Blavier, J.-F., Washenfelder, R., et al. (2023). TCCON data from Park Falls (US), Release GGG2020.R1 (Version R1) [Data set]. CaltechDATA. https://doi.org/10.14291/TCCON.GGG2020.PARKFALLS01.R1

Wong, K. W., Fu, D., Pongetti, T. J., Newman, S., Kort, E. A., Duren, R., et al. (2015). Mapping CH_4\$: CO_2\$ ratios in Los Angeles with CLARS-FTS from Mount Wilson, California. *Atmospheric Chemistry and Physics*, *15*(1), 241–252. https://doi.org/10.5194/acp-15-241-2015

Wunch, D., Toon, G. C., Blavier, J.-F. L., Washenfelder, R. A., Notholt, J., Connor, B. J., et al. (2011). The Total Carbon Column Observing Network. *Philosophical Transactions of the Royal Society A: Mathematical, Physical and Engineering Sciences*, *369*(1943), 2087–2112. https://doi.org/10.1098/rsta.2010.0240

Wunch, D., Toon, G. C., Hedelius, J. K., Vizenor, N., Roehl, C. M., Saad, K. M., et al. (2016). Quantifying the loss of processed natural gas within California's South Coast Air Basin using long-term measurements of ethane and methane. *Atmospheric Chemistry and Physics*, *16*(22), 14091–14105. https://doi.org/10.5194/acp-16-14091-2016

Wunch, D., Mendonca, J., Colebatch, O., Allen, N. T., Blavier, J.-F., Kunz, K., et al. (2023). TCCON data from East Trout Lake, SK (CA), Release GGG2020.R0 (Version R0) [Data set]. CaltechDATA. https://doi.org/10.14291/TCCON.GGG2020.EASTTROUTLAKE01.R0

Zeng, Z.-C., Pongetti, T., Newman, S., Oda, T., Gurney, K., Palmer, P. I., et al. (2023). Decadal decrease in Los Angeles methane emissions is much smaller than bottom-up estimates. *Nature Communications*, *14*(1), 5353. https://doi.org/10.1038/s41467-023-40964-w

Figure 1.

1830
1820
1810
1800
XCH$_4$ (ppb)
2016.0
2016.5
2017.0
2017.5
2018.0
2018.5
2019.0
original monthly mean
fitted monthly mean

Figure 2.

1880
1860
1840
1820
1800
1780
XCH$_4$ (ppb)
2016
2017
2018
2019
2020
2021
2022
2023

Figure 3.

y =(1.13±0.26)β + (-141.55±21.09)
XCH4 Monthly Anomalies (ppb)
40
30
20
10
0
−10
−20
2016
2017
2018
2019
2020
2021
2022
2023

Figure 4.


y =(1.16±0.21)β + (-109.7±22.62)
XCH4 Monthly Anomalies (ppb)
40
20
0
−20
−40
2016
2017
2018
2019
2020
2021
2022
2023

Figure 5.

120°W
60°W
0°
60°E
120°E
80°N
60°N
40°N
20°N
0°
20°S
40°S
1.4
1.2
1.0
0.8
0.6
0.4
0.2
0.0
Slope (ppb/month)

Figure 6.


CLARS fitted
OH -2%
OH -3%
OH -4%
OH -5%
OH -3% & CH4 +10Tg
OH -3% & CH4 +20Tg
OH -3% & CH4 +30Tg
XCH$_4$ monthly anomalies (ppb)
60
50
40
30
20
10
0
−10
−20
2016
2017
2018
2019
2020
2021
2022
2023

Figure A1.

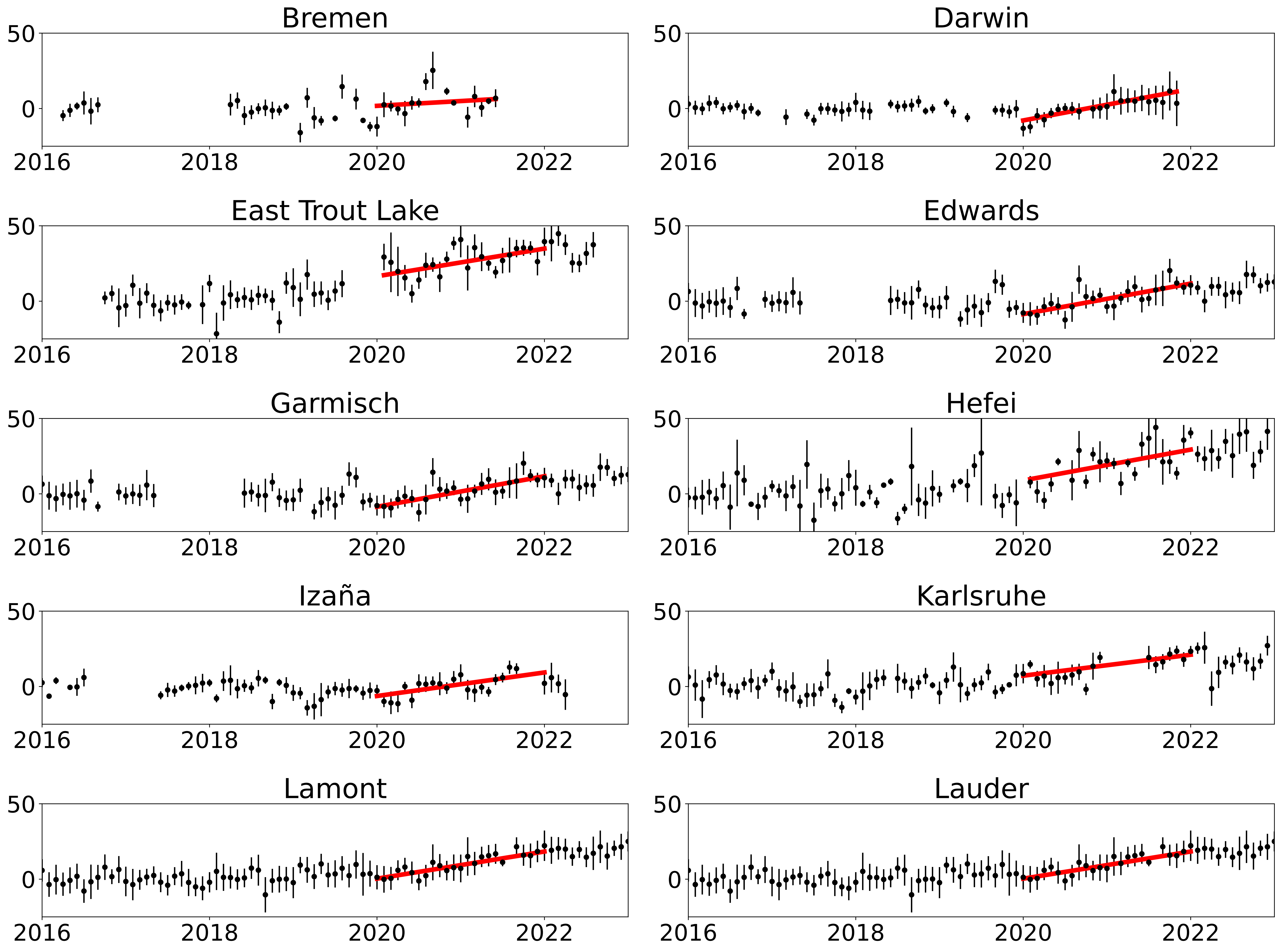
Bremen
Darwin
East Trout Lake
Edwards
Garmisch
Hefei
Izaña
Karlsruhe
Lamont
Lauder
50
0
2016
2018
2020
2022

Figure A2.

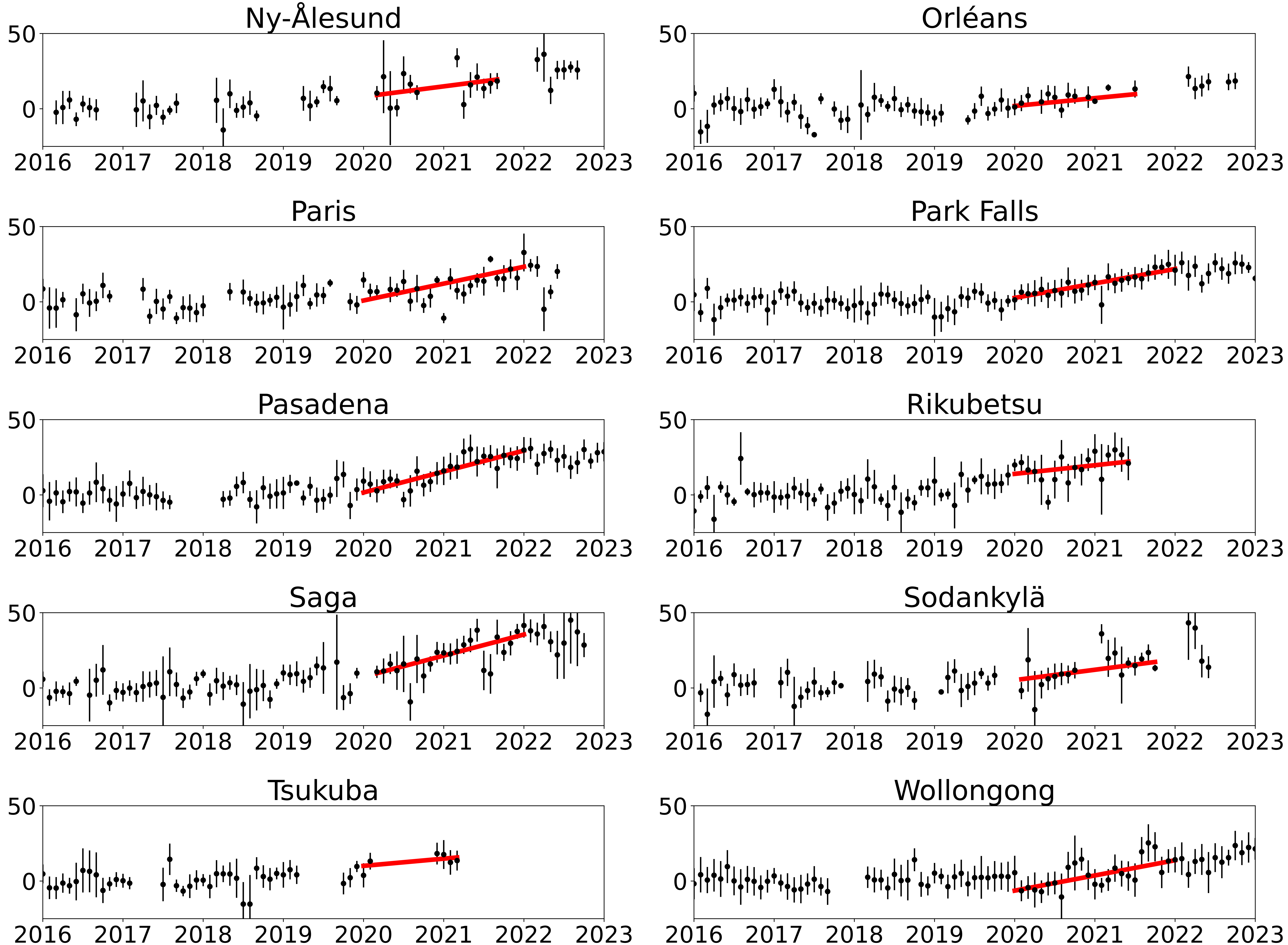

Ny-Ålesund
Orléans
Paris
Park Falls
Pasadena
Rikubetsu
Saga
Sodankylä
Tsukuba
Wollongong
50
0
2016
2017
2018
2019
2020
2021
2022
2023